Development of a ReaxFF potential for Ag/Zn/O and application to Ag deposition on ZnO

A. Lloyd[a,*], D. Cornil[b], A.C.T. van Duin[c], D. van Duin[c], R. Smith[a], S.D. Kenny[a], J. Cornil[b], D. Beljonne[b]

[a] *Loughborough University, Leicestershire, LE11 3TT, United Kingdom*
[b] *Laboratory for Chemistry of Novel Materials, University of Mons, 7000 Mons, Belgium*
[c] *RxFF Consulting, LLC, State College, PA 16801, United States*

Abstract

A new empirical potential has been derived to model an Ag-Zn-O system. Additional parameters have been included into the reactive force field (ReaxFF) parameter set established for ZnO to describe the interaction between Ag and ZnO for use in molecular dynamics (MD) simulations. The reactive force field parameters have been fitted to density functional theory (DFT) calculations performed on both bulk crystal and surface structures. ReaxFF accurately reproduces the equations of state determined for silver, silver zinc alloy and silver oxide crystals via DFT. It also compares well to DFT binding energies and works of separation for Ag on a ZnO surface. The potential was then used to model single point Ag deposition on polar $(000\bar{1})$ and non-polar $(10\bar{1}0)$ orientations of a ZnO wurtzite substrate, at different energies. Simulation results then predict that maximum Ag adsorption on a ZnO surface requires deposition energies of ≤ 10 eV.

Keywords: Density-functional calculations, Silver-zinc oxide interface, Reactive force field model, Surface adsorption energies, Ag deposition on ZnO, Molecular dynamics

1. Introduction

Silver has many scientific applications due to its high electrical and thermal conductivity [1] as well as its unique properties as an optical reflector [2, 3]. These properties make Ag perfect for coatings on solar cells and low-emissivity (Low-E) windows amongst other applications [4, 5]. Low-E coatings are used to reduce heat loss through windows via the reflection of infra red radiation. The reflective part of the coatings consist of a silver thin film applied to a seed layer. Zinc oxide is often chosen as the material for the seed layer due to its relatively low cost and semiconductor properties (having a wide band gap of 3.37 eV [6]) along with a reasonable propensity for Ag growth. There are many thin film layers applied to create a Low-E window coating - often including a tough, scratch resistant layer and an antireflective layer. However, the Ag/ZnO interface is known to be one of the weakest interfaces used within the reflective coating due to its low adhesive energy and large lattice mismatch ($\approx 11\%$) [7, 8]. An investigation of the adhesive properties of this interface and Ag growth could directly benefit the Low-E window industry. Any improvement in the production of this coating could reduce the amount of Ag used (reducing costs) and increase durability.

To model surface interactions and deposition events at an atomic scale, molecular dynamics (MD) [9] is often a method of choice. In MD simulations, all interatomic interactions are modelled by a potential function. The ReaxFF potential for zinc oxide [10] has proved to be useful in identifying growth mechanisms for ZnO by Blackwell *et al.* [11]. However, an existing Morse type potential for the Ag-ZnO interaction [12], fitted to reproduce works of separation, does not accurately predict binding energies.

The purpose of this work is to provide a model for Ag-ZnO interactions that encapsulates important surface characteristics. This model should provide binding energies for Ag on a ZnO surface similar to those found via DFT calculations whilst being computationally inexpensive (compared to DFT). The ReaxFF potential for Ag-ZnO interfaces has been produced and used to model deposition of Ag on polar $(000\bar{1})$ and non-polar $(10\bar{1}0)$ ZnO over an energy range from 0.1 to 30 eV, such as might be the case in magnetron sputtering [13, 14].

Previous modelling of ZnO polar surfaces suggest that O vacancies [15] could be present as a means of stabilising the polar $(000\bar{1})$ face. However, small scale structures used for fitting this model agree with experimental results indicating that the O-terminated polar face closely resembles the bulk termination [16] and that no defects other than $(10\bar{1}0)$ steps on the surface appear [17]. Growth has previously been studied on both polar $(000\bar{1})$-O terminated and (0001)-Zn terminated surfaces experimentally [18] as polar surfaces have been shown to be very stable [19]. This model has been fitted to the O-terminated $(000\bar{1})$ polar face, $(10\bar{1}0)$ non-polar face and several simple crystal structures, providing a range of structures which can be

*Corresponding author
Email address: a.lloyd3@lboro.ac.uk (A. Lloyd)

simulated accurately, because these surfaces were of more interest to our experimental collaborators.

2. Methodology

2.1. The ReaxFF Reactive Force Field

The Reactive Force Field (ReaxFF) potential, developed by van Duin *et al.* [20], depends on the bond order of atoms in a system. This potential has proven to be highly transferable, with an ability to describe both covalent, ceramic and metallic materials and their interfaces. The total energy of the system is expressed as a sum of bond order dependent and non-bonded energy terms (Eq. 1).

$$\begin{aligned} E_{system} = \quad & E_{bond} + E_{vdWaals} + E_{Coulomb} \\ & + E_{val} + E_{lp} + E_{tors} + E_{pen} \\ & + E_{conj} + E_{over} + E_{under}. \end{aligned} \tag{1}$$

E_{bond} represents the bond energy between atoms i and j. The potential can also take into account the valence angle terms (E_{val}), torsion angles ($E_{torsion}$), energy contributions associated with lone pairs, (E_{lp}), under and over coordination (E_{under} and E_{over}), additional energy penalties (E_{pen}) and possibly terms are included to account for conjugation effects. All these terms depend on bond order which in turn is determined via interatomic distances from the equation:

$$BO_{ij} \quad = BO^{\sigma}_{ij} + BO^{\pi}_{ij} + BO^{\pi\pi}_{ij} \tag{2}$$

where there are distinct differences between contributions from sigma, pi and double pi bonds,

$$\begin{aligned} BO^{\sigma}_{ij} \quad &= exp\left[P_{bo1}\left(\frac{r_{ij}}{r^{\sigma}_{o}}\right)^{P_{bo2}}\right] \\ BO^{\pi}_{ij} \quad &= exp\left[P_{bo3}\left(\frac{r_{ij}}{r^{\pi}_{o}}\right)^{P_{bo4}}\right] \\ BO^{\pi\pi}_{ij} \quad &= exp\left[P_{bo5}\left(\frac{r_{ij}}{r^{\pi\pi}_{o}}\right)^{P_{bo6}}\right]. \end{aligned} \tag{3}$$

Here BO_{ij} and r_{ij} represent the bond order and the interatomic distance between the ith and jth atom respectively. The r_o terms correspond to equilibrium bond lengths and P_{bo} terms are fitted bond parameters given in the supplementary material. The van der Waals and Coulomb ($E_{vdWaals}$ and $E_{Coulomb}$) terms are included for all pairs of atoms and are independent of bond order. The Coulomb interaction is modelled by a shielded Coulomb potential where atomic charges are calculated via the Electronegativity Equalization Method (EEM) [21].

For most systems, when creating a new parameter set for a ReaxFF potential, not all terms in Eq. (1) are deemed necessary. Keeping the number of terms down to a minimum, whilst maintaining a reasonable model, can decrease the computational time needed to run reliable simulations. As with the original parameter set for zinc oxide, many terms were set to zero yielding the reduced energy expression:

$$\begin{aligned} E_{system} = \quad & E_{bond} + E_{vdWaals} + E_{Coulomb} \\ & + E_{val} + E_{lp} + E_{over} + E_{under}. \end{aligned} \tag{4}$$

2.2. Fitting ReaxFF Parameters for Ag-Zn-O Systems

Equations of state for several crystal structures and binding energies were calculated by DFT using the SIESTA program [22]. To add Ag into the existing ZnO parameter set, Ag, Ag-Zn and Ag-O structures were examined. Cohesive energies were calculated for these lattices when undergoing uniform expansion and some selected distortions (see supplementary material). By using both expanded and distorted lattice configurations in the fitting procedure, bond distances and valence angle energies can be determined. First, simple cubic (SC), body centered cubic (BCC), face centered cubic (FCC) and hexagonal closed packed (HCP) structures for Ag were considered and compared to experimental data where available. To fit parameters for Ag-Zn interactions, three different atomic ratios were used in simple BCC and FCC structures. Ag_2O was considered in its natural cuprite crystal formation and is compared to other high symmetry AgO structures so as not to overestimate the stability of other oxidation states.

Additionally, adsorption energies were calculated for Ag atoms positioned on a polar $(000\bar{1})$ and non polar $(10\bar{1}0)$ ZnO surface, see Figure 1. The structures considered incorporated single Ag ad-atoms as well as Ag dimers and trimers positioned in various configurations on the surface. A range of these structures were used for the ReaxFF fitting procedure to help describe diffusion across the surface and find favourable adsorption sites. Subsurface Ag atoms were also considered when fitting the ReaxFF parameters to describe better the stability of Ag interstitials.

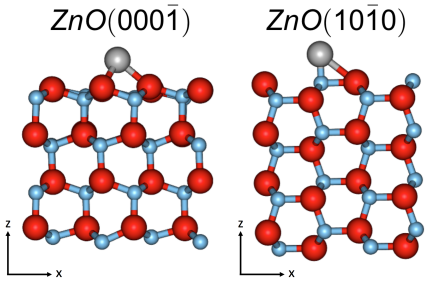

Figure 1: A schematic showing a single Ag ad-atom on the polar $(000\bar{1})$ and non polar $(10\bar{1}0)$ oriented ZnO wurtzite structure. Here, grey, red and blue spheres represent Ag, O and Zn atoms respectively.

Together with fixed parameters from the existing ZnO ReaxFF potential [23], the new parameter set was fitted by minimising the error:

$$\text{Error} = \sum_{i=1}^{n}\left[\frac{x_{i,DFT} - x_{i,RxFF}}{\sigma_i}\right]^2 \tag{5}$$

described by van Duin *et al.* [24]. In equation (5), $x_{i,DFT}$ and $x_{i,RxFF}$ are the DFT and calculated values respectively. The parameter σ_i corresponds to the weighting of data point i. Initial parameters were taken from the ReaxFF description of Cu/O/H [25] and then optimised against the DFT data.

2.3. Computational Details

The quantum-chemical calculations have been performed using Density Functional Theory through the SIESTA package. The treatment of exchange-correlation was done with the Perdew-Burke-Ernzerhof functional [26]. Valence electrons were described using a numerical DZP (double-zeta polarised) atomic basis set while Trouillier-Martins pseudopotentials were used for the description of the nuclei and core electrons [27]. Periodic boundary conditions were applied along the three directions of the space with dipolar corrections along the z-axis to cancel self-interaction between the cells. Equations of state for the smaller Ag and Ag-Zn crystal structures were sampled with a $12 \times 12 \times 12$ k-point sampling mesh of the Monkhorst-Pack type to compute the electronic structure in the Brillouin zone [28] with a mesh cutoff of 300 Ry. The slightly larger Ag-O crystal structures required a $8 \times 8 \times 8$ k-point sampling mesh with a larger cutoff of 600 Ry to match convergence. DFT calculations performed on the polar ZnO structure used a method of passivation of the Zn terminated face. This passivation was made by adsorption of OH on the Zn-terminated face.

For the ZnO surface, both the polar $(000\bar{1})$ and the non-polar $(10\bar{1}0)$ faces were considered with a similar surface per unit cell i.e. 9.75×11.26 Å for $(000\bar{1})$ and 10.40×9.74 Å for $(10\bar{1}0)$. Previous work has shown surface reconstruction due to the dipole moment however in our model the bottom Zn-terminated layer for the polar ZnO was passivated as in [29] and [30]. Here, a $3 \times 3 \times 1$ Monkhorst-Pack k-point grid was used with a slightly smaller, yet well converged, mesh cutoff of 250 Ry to reduce computation time. The relaxation of the silver atom and the two top ZnO layers were performed using the conjugate gradient method [31] until the forces acting on atoms were less than 0.04 eV/Å while the bottom layers were fixed in their bulk position.

The binding energy of the Ag atom on the ZnO surface was calculated using the expression:

$$E_{Bind} = [E_{Ag/ZnO} - E_{slab}^{ZnO} - n \cdot E_{bulk}^{Ag}]/n \qquad (6)$$

where $E_{Ag/ZnO}$ is the total energy of the relaxed Ag/ZnO surface, E_{slab}^{ZnO} the total energy of the relaxed ZnO surface and E_{bulk}^{Ag} the total energy of a single silver atom in bulk FCC conditions, see Table 1.

2.4. ReaxFF Molecular Dynamics

Deposition simulations via MD were conducted using the velocity Verlet algorithm [32] with a corresponding time step of 1 fs. Periodic boundaries were implemented in the x and y directions along with a fixed bottom ZnO layer to emulate a large ZnO slab. A Berendsen thermostat [33] is used for temperature control applied to the second and third double ZnO layers. The simulation cells used for the polar and non-polar ZnO surfaces were of similar volume, namely $22.80 \times 26.33 \times 30$ Å (with 512 atoms) for ZnO $(000\bar{1})$ and $26.51 \times 26.33 \times 30$ Å (with 640 atoms) for ZnO $(10\bar{1}0)$.

Table 1: Comparison of lattice parameters and cohesive energies from DFT, ReaxFF and experimental results where available for Ag structures. (Experimental results were taken for AgZn at room temperature, Ag_2O at 40 K and Ag FCC at room temperature and 0 K for lattice constant and cohesive energy respectively.)

Structure	Property	DFT	ReaxFF	Exp
Ag SC	a/Å	2.78	2.97	
	E_{Coh}/eV	-2.53	-2.45	
Ag FCC	a/Å	4.19	4.22	4.09 [34]
	E_{Coh}/eV	-2.91	-3.04	-2.95 [34]
Ag BCC	a/Å	3.33	3.33	
	E_{Coh}/eV	-2.90	-3.00	
Ag HCP	a/Å	2.97	3.00	
	c/Å	4.83	4.89	
	E_{Coh}/eV	-2.90	-3.04	
Ag_3Zn FCC	a/Å	4.11	4.12	
	E_{Coh}/eV	-2.63	-2.77	
AgZn BCC	a/Å	3.20	3.22	3.16 [35]
	E_{Coh}/eV	-2.36	-2.39	
$AgZn_3$ FCC	a/Å	3.98	3.96	
	E_{Coh}/eV	-2.02	-1.99	
Ag_2O Cuprite	a/Å	4.85	4.87	4.75 [36]
	E_{Coh}/eV	-3.78	-3.76	
AgO Rocksalt	a/Å	4.70	4.69	
	E_{Coh}/eV	-4.09	-4.62	
AgO Sphalerite	a/Å	5.10	5.08	
	E_{Coh}/eV	-3.88	-3.91	

3. Results and Discussion

The objective for this fitted parameter set is to reproduce equations of state (EoS) for a number of crystal structures and give binding energies for different surface structures with reasonable accuracy.

3.1. Equations of State

For this parameter set to be successful at modelling the surface interaction and growth, DFT and ReaxFF must exhibit a good agreement for cohesive energies and lattice constants. Table 1 shows that the ReaxFF is fitted well to these conditions and is also in good agreement with experimental data for available structures. The largest error occurs for the AgO Rocksalt polymorph with a cohesive energy difference between DFT and ReaxFF at equilibrium of 13%.

As shown in Figure 2, ReaxFF reproduces very well the equations of state found by DFT. Cohesive energies match for nearly all structures considered. For the pure Ag crystal structures, the energetically favourable configurations fit almost perfectly to the DFT data. The curve

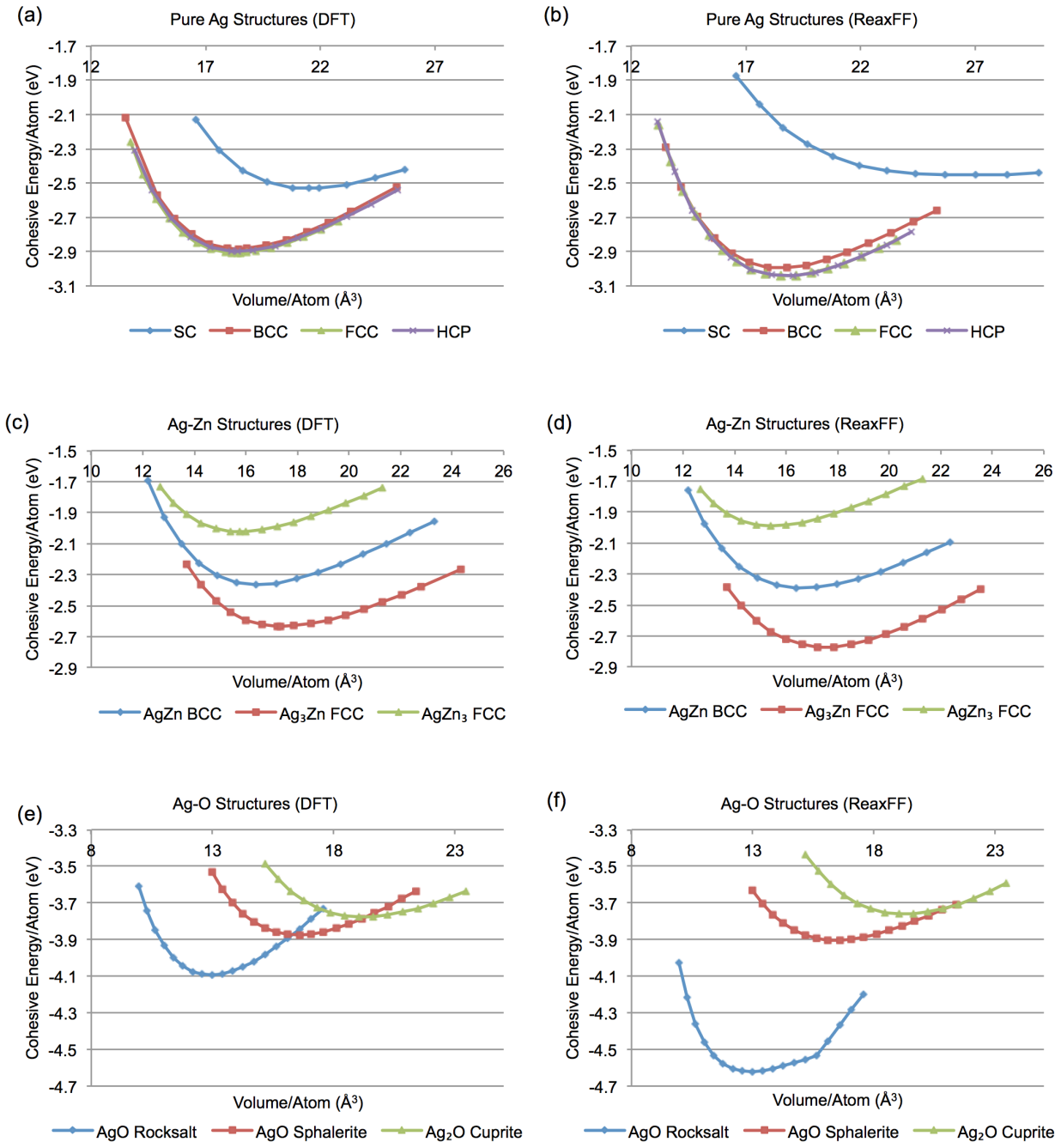

Figure 2: Equations of state for silver, (a) and (b), silver-zinc, (c) and (d), and silver-oxygen, (e) and (f), crystal structures when undergoing uniform expansion. The plots (a), (c) and (e) show the equations of states as calculated via DFT. The plots (b), (d) and (f) show the equations of state as calculated via ReaxFF for comparison.

for the simple cubic structure is poorly matched but is very high in energy - as such, this disagreement is believed to be acceptable since it will not impact growth simulations. Note that for the HCP structure, the c/a ratio was kept constant at 1.63. Cohesive energies for all three Ag-Zn alloy structures, are also consistent with the DFT data. For silver oxides, the favourable AgO rocksalt is made more stable whilst AgO sphalerite and Ag_2O cuprite remain similar when comparing the ReaxFF and DFT data. The one slight concern here is the over stability of the rocksalt polymorph and the deviation in the curve though this does not change the relative stability of the three phases. Reducing the stability of the rocksalt polymorph would be at the expense of more accurate surface results.

Equations of state were also compared for a selection of distorted lattice structures, namely for pure Ag in FCC and BCC structures, AgZn in BCC, Ag_3Zn and $AgZn_3$ in

FCC, AgO in rocksalt and Ag_2O in a cuprite structure (see supplementary material). The equilibrium lattice parameters found during the uniform expansion calculations were multiplied by 1-δ in 2 directions and by 1+δ in the other direction. Here, δ is the distortion parameter with values varying from -0.1 to 0.1.

3.2. Binding Energies

An important task for the ReaxFF parameter set for our interest is to recreate binding energies and bonding sites for small silver clusters on and just below the ZnO polar and non-polar surfaces. DFT results, shown in Figure 3, show a relatively high binding energy for Ag on the polar ZnO surface, implying that a high proportion of Ag atoms will stick to the surface after deposition rather than reflect. However, this seems less likely for the non-polar surface in view of the lower binding energies. Thus, accurate adsorption energies are needed for reliable single point deposition statistics. After deposition events, diffusion of Ag across the surface has to then be considered. Hence, energy differences between different adsorption sites and positions for Ag atoms must be consistent with the DFT results.

In general, the ReaxFF potential reproduces the binding energies of Ag on the polar and non-polar ZnO surface calculated via DFT well. However, there is a slight tendency for the potential to underestimate the magnitude of the binding energy for the majority of the structures with the exception of one of the interstitial structures. In Figure 3, structures are categorised into polar surface and non-polar surface to indicate the ZnO surface orientation and 3 structures including subsurface Ag atoms on a polar ZnO substrate are labeled as interstitials. The least favourable interstitial structure describes an Ag atom positioned ~4 Å deep into the ZnO surface between O and Zn layers. The structure is energetically unfavourable when calculated via ReaxFF compared to other structures examined. However, this is not a concern when simulating low energy deposition simulations as this structure is highly unlikely to occur. The other two interstitial cases describe an Ag atom situated below the first O and Zn layer in a hollow site and below a Zn atom. It is also worth noting that both the DFT and ReaxFF results indicate that it is energetically favourable for Ag adatoms to be dispersed seperately across the polar surface. In contrast, Ag prefers to form clusters on the non-polar surface.

3.3. Works of Separation

In order to test the potential further, the work of separation of the Ag-ZnO interface was calculated and compared to previous DFT calculations from the literature [8]. A coherent (1×1) Ag(111)/ZnO(000$\bar{1}$) interface was considered. To achieve the coherent interface, the Ag lattice was stretched laterally to match the lattice constant of ZnO. 6 layers of Ag (111) positioned above 4 double layers of ZnO(000$\bar{1}$) in three high symmetry adsorption sites, see Figure 4, were considered with a surface area, A, of 600 Å^2. The outermost 2 layers of silver and 2 double layers of ZnO were fixed, such that the interface spacing was optimal, then atoms near the interface were relaxed. Works of separation, W_{sep}, were then calculated via

$$W_{sep} = (E^{Ag}_{slab} + E^{ZnO}_{slab} - E_{Ag/ZnO})/A. \quad (7)$$

and compared to DFT values, see Table 2. In eq. (7), $E_{Ag/ZnO}$ is the total energy of the relaxed structure whilst E^{Ag}_{slab} and E^{ZnO}_{slab} represent the energy of the isolated relaxed structures of the pure Ag and ZnO slabs respectively. Despite the ReaxFF parameter set not being fitted to works of separation, Table 2 shows a very good agreement between ReaxFF and the DFT values from the literature.

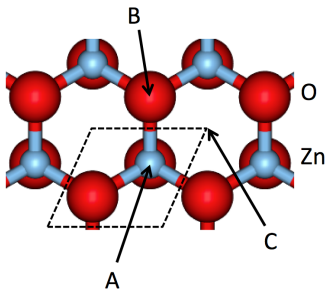

Figure 4: The high symmetry adsorption sites on the (000$\bar{1}$) ZnO surface considered when calculating W_{sep}.

Table 2: Works of Separation, W_{sep} and interlayer spacing (d_{Ag-O}) calculated for the (1×1) coherent Ag/ZnO interface. The Ag slab was positioned in 3 different adsorption sites then near interface atoms were relaxed. DFT values found by Lin and Bristowe [8] are in brackets.

Adsorption site	W_{sep} (J/m^2)	d_{Ag-O} (Å)
A	0.68 (0.74)	2.41 (2.31)
B	1.44 (1.40)	2.30 (2.30)
C	0.67 (0.83)	2.40 (2.14)

4. Application: Single Point Depositions

As a precursor to considering how Ag grows on the ZnO surface, the interaction of Ag atoms and Ag_2 dimers with a ZnO surface was investigated. A study into how Ag deposits onto a ZnO substrate at different depositions energies (ranging from 0.1 to 30 eV) has been carried out via MD simulations. Ag atoms were deposited normal to the surface over the regions shown in Figure 5. Each Ag atom is initially placed over 10 Å above the surface outside of the ReaxFF cutoff. Here, a sample of 400 separate simulations have been run for each of the 5 deposition energies with the initial atom or dimer placed above the surface. For Ag_2 dimer deposition, the dimer is randomly

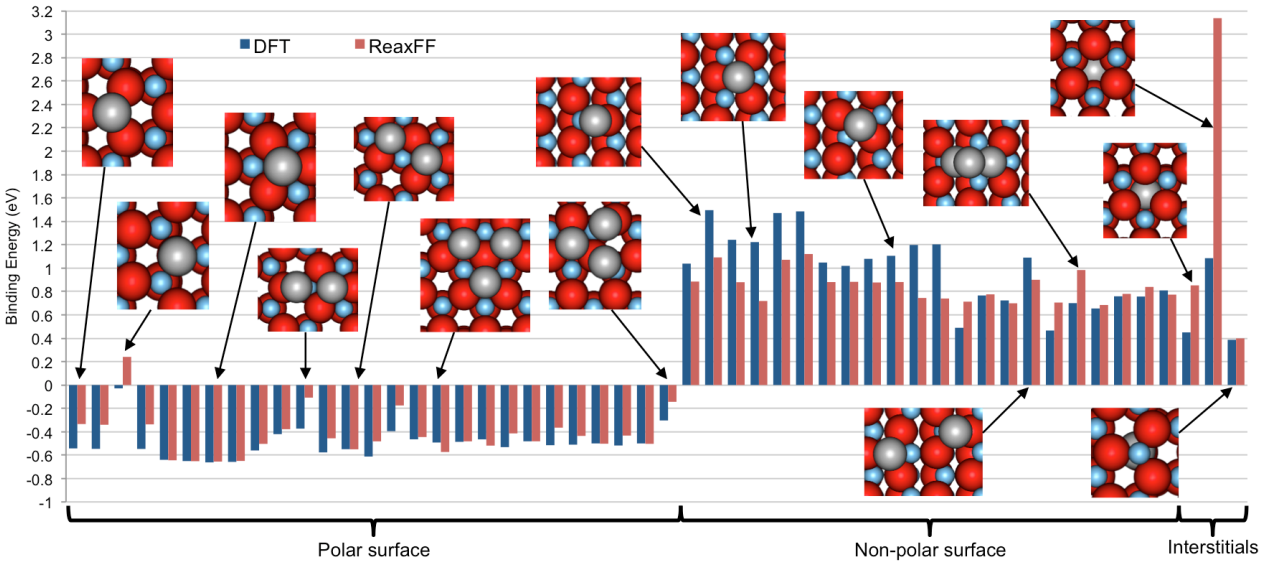

Figure 3: A comparison of the binding energies calculated from DFT and ReaxFF for all structures used in the fitting procedure. Example structures are shown alongside their corresponding calculated binding energies. The fitted potential captures the trends in binding energies well.

orientated before deposition is undergone. In a typical Ag deposition event, a single Ag atom gains a charge of 0.6 $|e|$ as it approaches the polar ZnO surface. This charge transfer promotes Ag-O bonding on the polar surface.

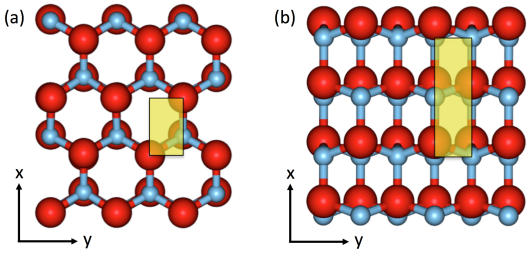

Figure 5: Schematic of the irreducible symmetric zone considered for deposition of Ag on the (a) polar and (b) non polar ZnO surface.

The results shown in Tables 3, 4, 5 and 6 have been categorised into 3 different outcomes: namely adsorb, penetrate and reflect. These labels are sufficient to describe low energy impacts of Ag onto the ZnO. The term split in tables 4 and 6 refers to the case when the incoming Ag_2 dimer breaks apart on impact. However, for higher energy deposition simulations (>30 eV), more categories may be needed to describe surface damage caused by Ag collisions.

4.1. Ag on ZnO $(000\bar{1})$

The previous calculations indicate that the polar ZnO surface is energetically favourable for Ag adsorption.

For Ag monomer depositions on the polar surface, atoms penetrate only once the deposition energy reaches 30 eV. Deposition events with an energy of $\leq$ 10 eV always result in adsorption onto the surface and around 70% adsorb at energies around 30 eV (while 30% penetrate). Similar results were seen for Ag dimer depositions. It is not until deposition energies increase to around 30 eV that there were penetrating Ag atoms (in this case 92.5% of deposited atoms still adsorb to the surface). For all energies in the range considered, around one third of all dimers deposited split into 2 Ag monomers during the deposition event. Note also, no Ag atoms reflect during these deposition simulations. Figure 6 shows the final resting place of the Ag atoms after impact for energies of 0.1 and 10 eV.

Table 3: Single Ag deposition on ZnO $(000\bar{1})$

	Deposition Energy (eV)				
Outcome	0.1	1	3	10	30
Adsorb (%)	100	100	100	100	70
Penetrate (%)	0	0	0	0	30

Table 4: Ag dimer deposition on ZnO $(000\bar{1})$

	Deposition Energy (eV)				
Outcome	0.1	1	3	10	30
Adsorb (%)	100	100	100	100	92.5
Penetrate (%)	0	0	0	0	7.5
Split (%)	32	32.5	29.5	45.5	38

4.2. Ag on ZnO $(10\bar{1}0)$

The other surface considered is the non-polar $(10\bar{1}0)$ orientation of ZnO. In general, the Ag binding energies on

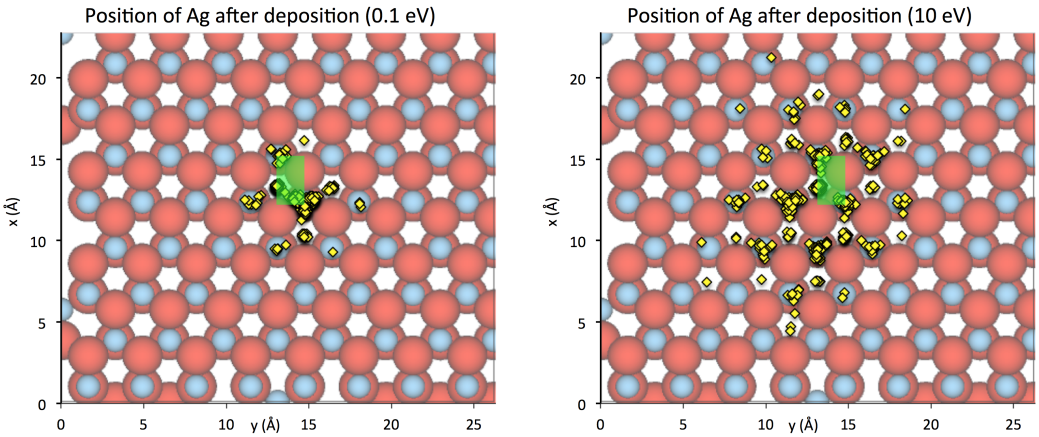

Figure 6: Plots showing final positions of single Ag atoms deposited at 0.1 and 10 eV on a ZnO $(000\bar{1})$ substrate after 10 ps. Yellow diamonds indicate final position of Ag atoms and the green rectangle shows the deposition area. As one would expect, the higher the deposition energy the more the Ag atoms tend to move across the surface. Once Ag atoms are deposited, the atoms then bond to either an A (above a Zn atom) or C (hollow) adsorption site.

this surface are much weaker than on the polar surface. Results are tabulated in Tables 5 and 6.

Table 5: Single Ag deposition on ZnO $(10\bar{1}0)$

	Deposition Energy (eV)				
Outcome	0.1	1	3	10	30
Adsorb (%)	100	100	100	99.25	69.25
Penetrate (%)	0	0	0	0.25	30.75
Reflect (%)	0	0	0	0.5	0

Table 6: Ag dimer deposition on ZnO $(10\bar{1}0)$

	Deposition Energy (eV)				
Outcome	0.1	1	3	10	30
Adsorb (%)	100	100	100	99.75	89
Penetrate (%)	0	0	0	0.25	9.5
Reflect (%)	0	0	0	0	1.5
Split (%)	3.5	9	18	25.5	19

Ag atoms start to penetrate the target surface with deposition energies of 10 eV (much lower than for the polar surface). On the non-polar surface, Ag monomer and dimer depositions yield very similar results with 69% of deposited atoms result in adsorption at 30 eV (which the majority of other atoms penetrating the surface). For deposition energies of less than 10 eV however, all Ag atoms adsorb. There are also cases of reflected atoms at 10 and 30 eV whereas none were reflected in the case of the polar surface. Note that the tendency for dimers to split is less marked than for the polar surface. This is due to Ag atoms in cluster formations being energetically favourable on the non-polar surface. Figure 7 shows the final resting place of the Ag atoms after impact for energies of 0.1 and 10 eV.

5. Conclusions

A new potential to describe the Ag-ZnO system has been developed. The new parameters were fitted against DFT calculations with the aim of reproducing equations of state for simple crystal structures and Ag on ZnO binding energies. Overall, the fitted parameter set agrees well with the DFT data used within the fitting procedure as well as agreeing with experimental data and calculated works of separation. As a preliminary phase to undertaking growth simulations [37], single point depositions onto a perfect ZnO surface were also carried out. All low energy depositions (below 30 eV) of Ag onto perfect polar ZnO resulted in adsorption. Similar results were seen when depositing on the non-polar ZnO surface. Ag atoms do not penetrate the surface until energies of 10 eV or more are used. No reflection was seen on the polar surface in contrast to the non-polar case, where a small fraction of reflected atoms is predicted. This indicates that in magnetron sputtering deposition it may be better to use lower deposition energies if a sharp interface between the Ag film and the ZnO substrate is to be maintained.

In practice, foreign adsorbents (including H and water molecules) may be found on the surface during the deposition process but are not considered in this potential. It could be possible to include some contaminates in the ReaxFF potential but this would affect efficiency.

Acknowledgments

The research at Loughborough was supported by EPSRC, AGC Glass Europe and the Loughborough HPC unit. The work in Mons was supported by the Région Wallonne, (Aide à la subvention - Project 7189 with AGC

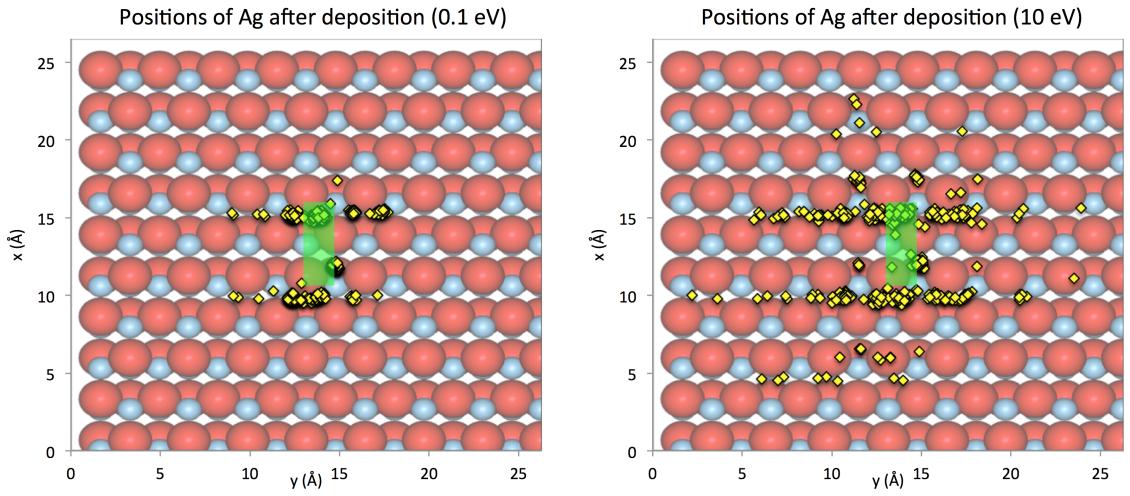

Figure 7: Plots showing final positions of single Ag atoms deposited at 0.1 and 10 eV on a ZnO $(10\bar{1}0)$ substrate after 10 ps. Yellow diamonds indicate final position of Ag atoms and the green rectangle shows the deposition area. Again, the higher the deposition energy the more the Ag atoms tend to move across the surface. Ag atoms favour bonding sites away from surface Zn atoms.

Glass Europe) and the Belgian National Fund for Scientific Research. J.C. and D.B. are FNRS research directors. The authors would like the thank Hugues Wiame and Benoit Lecomte for useful discussions.

References

[1] G. Kaye, T. Laby, Tables of Physical and Chemical Constants, 16th Edition, Longman, Harlow, 1995.

[2] A. Rakić, A. Djurišić, J. Elazar, M. Majewski, Optical properties of metallic films for vertical-cavity optoelectronic devices, Appl. Opt. 37 (22) (1998) 5271–5283.

[3] G. Hass, Filmed surfaces for reflecting optics, J. Opt. Soc. Am. 45 (11) (1955) 945–952.

[4] R. Hummel, K. Guenther (Eds.), Handbook of Optical Properties: Thin Films for Optical Coatings, Vol. 1, CRC, Boca Raton, FL, 1995.

[5] H. Glaser, History of the development and industrial production of low thermal emissivity coatings for high heat insulating glass units, Appl. Opt. 47 (13) (2008) c193–c199.

[6] Z. Wang, Zinc oxide nanostructures: growth, properties and applications, J. Phys. Condens. Matter 16 (2004) R829–R858.

[7] E. Barthel, O. Kerjan, P. Nael, N. Nadaud, Asymmetric silver to oxide adhesion in multilayers deposited on glass by sputtering, Thin Solid Films 473 (2005) 272–277.

[8] Z. Lin, P. D. Bristowe, Microsopic characteristics of Ag(111)/ZnO(0001) interface present in optical coatings, Phys. Rev. B 75 (2007) 205423.

[9] R. Smith (Ed.), Atomic and ion collisions in solids and at surfaces: theory, simulation and applications, Cambridge University Press, 1997.

[10] D. Raymand, A. van Duin, M. Baudin, K. Hermansson, A reactive force field (ReaxFF) for zinc oxide, Surf. Sci. 602 (2008) 1020–1031.

[11] S. Blackwell, R. Smith, S. Kenny, J. Walls, C. Sanz-Navarro, Modelling the growth of ZnO thin films by PVD methods and the effects of post-annealing, J. Phys. Condens 25 (13) (2013) 135002.

[12] I. Gheewala, S. Kenny, R. Smith, Atomistic-scale modelling of nano indentation into optical coatings, Philos. Mag. 89 (34-36) (2009) 3499–3510.

[13] K. Seshan (Ed.), Handbook of Thin Film Deposition Processes and Techniques: principles, methods, equipment and applications, Noyes Publications, 2002.

[14] K. Chopra, I. Kaur, Thin Film Device Applications, Plenum Press, 1983.

[15] R. Wahl, J. V. Lauritsen, F. Besenbacher, G. Kresse, Stabilization mechanism for the polar ZnO$(000\bar{1})$-O surface, Phys. Rev. B 87 (2013) 085313.

[16] M. Galeotti, A. Atrei, U. Bardi, G. Rovida, M. Torrini, E. Zanazzi, A. Santucci, A. Klimov, Structure of ZnO$(000\bar{1})$ surface studied by X-ray photoelectron diffraction, Chem. Phys. Lett. (1994) 349–352.

[17] T. M. Parker, N. G. Condon, R. Lindsay, F. M. Leibsle, G. Thornton, Imagining the polar $(000\bar{1})$ and non-polar $(10\bar{1}0)$ surfaces of ZnO with STM, Surf. Sci. 415 (3) (1998) L1046–L1050.

[18] L. V. Koplitz, O. Dulub, U. Diebold, STM study of copper growth on ZnO(0001)-Zn and ZnO$(000\bar{1})$-O surfaces, J. Phys. Chem. B 107 (2003) 10583–10590.

[19] A. Wander, F. Schedin, P. Steadman, A. Norris, R. McGrath, T. S. Turner, G. Thornton, N. M. Harrison, Stabilty of polar oxide surfaces, Phys. Rev. Lett. 86 (17) (2001) 3811–3814.

[20] A. van Duin, S. Dasgupta, F. Lorant, W.A. Goddard III, ReaxFF: a reactive force field for hydrocarbons, J. Phys. Chem. A, 105 (41) (2001) 9396–9409.

[21] W. Mortier, S. Ghosh, S. Shankar, Electronegativity equalization method for the calculation of atomic charges in molecules, J. Am. Chem. Soc. 108 (1986) 4315–4320.

[22] J. Soler, E. Artacho, J. Gale, A. García, J. Junquera, P. Ordejón, D. Sánchez-Portal, The SIESTA method for ab initio order-N materials simulation, J. Phys. Condens. Matter 14 (2002) 2745–2779.

[23] D. Raymand, A. van Duin, D. Spånberg, W.A. Goddard III, K. Hermansson, Water adsorption on stepped ZnO surfaces from MD simulations, Surf. Sci. 604 (2010) 714–752.

[24] A. van Duin, J. Baas, B. van de Graaf, Delft molecular mechanics:a new approach to hydrocarbon force fields, J. Chem. Soc. Faraday Trans. 90 (19) (1994) 2881–2895.

[25] A. van Duin, V. Bryantsev, M. Diallo, W. Goddard, O. Rahaman, D. Doren, D. Raymand, K. Hermansson, Development and validation of a ReaxFF reactive force field for Cu cation/water interactions and copper metal/metal oxide/metal hydroxide condensed phases, J. Phys. Chem. A 114 (35) (2010) 9507–9514.

[26] J. Perdew, K. Burke, M. Ernzerhof, Generalized gradient approximation made simple, Phys. Rev. Lett. 77 (18) (1997) 3865.

[27] N. Troullier, J. Martins, Efficient pseudopotentials for plane-wave calculations, Phys. Rev. B 43 (3) (1993) 1993–2006.

[28] H. Monkhorst, J. Pack, Special points for Brillouin-zone integrations, Phys. Rev. B 13 (12) (1976) 5188–5192.
[29] D. Cornil, T. van Regemorter, D. Beljonne, J. Cornil, Work function shifts of a zinc oxide surface upon deposition of self-assembled monolayers: a theoretical insight, Phys. Chem. Chem. Phys. 16 (2014) 20887–20899.
[30] H. Li, L. K. Schirra, J. Shim, H. Cheun, B. Kippelen, O. L. A. Monti, J. Bredas, Zinc oxide as a model transparent conducting oxide: A theoretical and experimental study of the impact of hydroxylation, vacancies, interstitials, and extrinsic doping on the electronic properties of the polar ZnO (0002) surface, Chem. Mater. 24 (2012) 3044–3055.
[31] R. Fletcher, C. Reeves, Function minimizaton by conjugate gradients, Comput. J. 7 (1964) 149–154.
[32] L. Verlet, Computer 'experiments" on classical fluids. I. Thermodynamical properties of Lennard-Jones molecules, Phys. Rev. 159 (1967) 98–103.
[33] H. Berendsen, J. Postma, W. van Gunsteren, A. DiNola, J. Haak, Molecular dynamics with coupling to an external bath, J. Chem. Phys. 81 (8) (1984) 3684–3690.
[34] C. Kittel, Introduction to Solid State Physics, 8th Edition, Wiley, 2004.
[35] W. Pearson, A Handbook of Lattice Spacings and Structures of Metals and Alloys, Pergamon Press, London, 1958.
[36] T. Lin, C. Li, J. Niedziela, H. Smith, D. Abernathy, G. Rossman, B. Fultz, Anharmonic lattice dynamics of Ag2O studied by inelastic neutron scattering and first principles molecular dynamics simulations, Phys. Rev. B 89 (2014) 054306.
[37] C. Scott, S. Blackwell, L. Vernon, S. Kenny, M. Walls, R. Smith, Atomistic surface erosion and thin film growth modelled over realistic time scales, J. Chem. Phys. 135 (2011) 174706.